



**Diffusion of multiple electrolytes cannot be treated independently: Model predictions with experimental validation**

|                               |   |
|-------------------------------|---|
| Journal:                      | <i>Soft Matter</i>  |
| Manuscript ID                 | SM-ART-09-2019-001780.R1  |
| Article Type:                 | Paper   |
| Date Submitted by the Author: | 18-Oct-2019   |
| Complete List of Authors:     | Gupta, Ankur; Princeton University, Department of Mechanical and Aerospace Engineering<br>Shim, Suin; Princeton University, MAE<br>Issah, Luqman; Princeton University, Department of Chemical Engineering<br>McKenzie, Cameron; Princeton University, Department of Chemical Engineering<br>Stone, Howard; Princeton, Mechanical and Aerospace Engineering |
|                               |   |

Cite this: DOI: 00.0000/xxxxxxxxxx

## Diffusion of multiple electrolytes cannot be treated independently: Model predictions with experimental validation<sup>†</sup>

Ankur Gupta,<sup>a</sup> Suin Shim,<sup>a</sup> Luqman Issah,<sup>b</sup> Cameron McKenzie,<sup>b</sup> and Howard A. Stone<sup>\*a</sup>

Received Date

Accepted Date

DOI: 00.0000/xxxxxxxxxx

We study the diffusion of multiple electrolytes in a one-dimensional pore. We model the scenario where an electrolyte is in contact with a reservoir of another electrolyte, such that the cation of the two electrolytes is common. The model reveals that several factors influence the ion concentration profiles: (i) relative diffusivities of the ions, (ii) ratio of the electrolyte concentrations in the pore and the reservoir, and (iii) the valence of the ions. We demonstrate that it is crucial to consider the interaction between ion fluxes as treating the electrolytes independently, as is sometimes proposed, does not completely capture the dynamics of ion transport. We validate our numerical predictions by conducting experiments with sodium fluorescein salt in the pore and sodium chloride / sodium sulphate / sodium hydroxide in the reservoir. Our visualization and results demonstrate that ion diffusivities and concentrations in the reservoir can influence the diffusion rates of fluorescein, which underscores that ion fluxes are coupled and that multiple electrolytes cannot be treated independently. These results should be useful to the wide range of situations where concentration variations are imposed on systems with an existing background electrolyte.

### 1 Introduction

From biological fluids such as blood and urine, to energy storage devices such as batteries and supercapacitors, electrolytes play a pivotal role in human life. In several of these physical systems, fluid phases may contain multiple electrolytes with varying concentrations, ion diffusivities and valences. For instance, human blood consists of  $\text{Ca}^{2+}$ ,  $\text{K}^+$ ,  $\text{Na}^+$ ,  $\text{Cl}^-$ ,  $\text{PO}_4^{3-}$ , among others.

The majority of studies on electrolyte transport focus on a single binary electrolyte<sup>1–5</sup>. However, a few prior reports discuss the transport of multiple electrolytes in cement pores<sup>6–10</sup>, ion exchange and electrochemical processes<sup>4,11–14</sup>, and diffusion measurement studies<sup>15–17</sup>. Recently, several microfluidic studies have also acknowledged the importance of multiple electrolytes to manipulate colloidal transport via electrokinetic processes such

as electrophoresis and diffusiophoresis<sup>18–29</sup>. In this article, we focus on understanding and quantifying the diffusive transport in ionic solutions that contain multiple electrolytes by employing both experimental and theoretical techniques.

There is a large body of literature for an electroneutral binary electrolyte, where the effective diffusivity of the ions is given by the ambipolar diffusivity<sup>1–4</sup>. Physically, the ambipolar diffusivity ensures that if the cation and anion of an electrolyte have different diffusivities, the faster moving ion is slowed in order to satisfy the electroneutrality condition. In the same spirit, we seek to determine the factors that control the ionic transport of a electroneutral mixture of two binary electrolytes. Though some earlier studies have reported results for multiple electrolytes under conditions of electroneutrality<sup>4,8,9,13,14</sup>, the analysis is typically system specific and/or dimensional, which limits the applicability. In addition, several of these studies are numerical and lack experimental validation.

We consider a physical scenario where electrolyte A is brought in contact with a reservoir of electrolyte B; see Fig. 1(a). For simplicity, we assume that electrolytes A and B have a common cation and allow for arbitrary diffusivities of the cations and anions. We emphasize that when the diffusivity ratios of cations and anions are large, the dynamics of ion transport become highly coupled. For example, we conduct experiments with sodium

<sup>a</sup> Department of Mechanical and Aerospace Engineering, Princeton University, Princeton NJ 08544 USA

<sup>b</sup> Department of Chemical and Biological Engineering, Princeton University, Princeton NJ 08544 USA

\* To whom the correspondence should be addressed, hastone@princeton.edu

† Electronic Supplementary Information (ESI) available: [details of any supplementary information available should be included here]. See DOI: 00.0000/00000000.

fluorescein as electrolyte A and sodium hydroxide as electrolyte B, where the diffusivity of hydroxide ions is much larger than the diffusivities of sodium and fluorescein ions. As we show later, the dynamics of fluorescein ion transport is significantly influenced by the presence of hydroxide ions.

There are two possible approaches to predict the transport of electrolytes A and B (Fig. 1(b)): (i) assume that the electrolytes are independent of each other, an approach employed due to its simplicity<sup>2,22</sup>, and (ii) a more rigorous approach where all the ionic fluxes are coupled due to electroneutrality. In the first method, the cations and anions of electrolyte A diffuse as if there is no electrolyte B, and vice-versa. Therefore, the electrolytes satisfy the electroneutrality condition *individually* (Fig. 1(b)). In contrast, the second method only enforces that the electroneutrality is satisfied *collectively* (Fig. 1(b)).

We now qualitatively compare the predictions of the two methods for a scenario when the diffusivity of anions of electrolyte B is much larger than the other two ions. For this specific scenario, the independent electrolyte analysis predicts a slower diffusion rate for anions of electrolyte B as compared to the coupled analysis since the anions of electrolyte B can satisfy electroneutrality only with the cations of electrolyte B; see Fig. 1(c). In this article, we demonstrate both theoretically and experimentally that it is important to employ the second approach to correctly capture the diffusive transport of ions, especially when the diffusivity contrast between ions is significant. Furthermore, we also investigate the effect of electrolyte concentration on the diffusion of ions.

In Section 2, we describe the details of a microfluidic setup with a sodium fluorescein salt to experimentally measure by direct visualization the evolving concentration profiles in configurations with a common cation. In Section 3, we provide the details of our mathematical model where we compare and contrast the two approaches for multiple electrolytes (*i.e.*, the analysis assuming electrolytes are independent and the analysis where ion fluxes are coupled). Next, we compare the predictions of the coupled model and the independent model with the experimental results in Section 4. Lastly, we discuss the implication of our findings and directions for future research in Section 5.

## 2 Experimental methods

We use a dead-end pore geometry<sup>30,31</sup> to experimentally study the diffusion of multiple electrolytes. The dead-end pore channels are prepared by standard soft lithography with the monomer to crosslinker ratio 10:1. The width, height, and the length of the main channel and the pores, respectively, are  $W = 750 \mu\text{m}$ ,  $H = 150 \mu\text{m}$  and  $L = 5 \text{ cm}$ , and  $w = 100 \mu\text{m}$ ,  $h = 50 \mu\text{m}$  and  $\ell = 1 \text{ mm}$  (Fig. 2).

We initially fill the dead-end pores with 2 mM sodium fluorescein (FSS) solutions, a disodium salt. Next, we introduce an air bubble into the main channel at a volumetric flowrate of 350  $\mu\text{L/hr}$ , which is followed by the second electrolyte solution, *i.e.*, 0.4 mM NaCl / 2 mM  $\text{Na}_2\text{SO}_4$  / 4 mM NaOH; see Fig. 2(a). Once the two electrolyte solutions come in contact with each other, the mean flow rate is reduced to 20  $\mu\text{L/hr}$ , corresponding to a mean flow speed  $\langle u \rangle = 50 \mu\text{m/s}$ . All solutions are loaded

by a syringe pump (Harvard Apparatus).

In order to prevent photobleaching of fluorescein<sup>32</sup> (see Supporting Information), we set up the experiments under the brightfield mode of the inverted microscope (Leica DMI4000B). Once the two electrolyte solutions contact each other, we switch the microscope to the fluorescent mode and take images at 7 ms exposure and 1-minute intervals. As a result, we obtain a time sequence of images visualizing the concentration profile of fluorescein in the pores (Fig. 2(b)).

For image analysis, we fix the region of interest (ROI, 80  $\mu\text{m} \times 990 \mu\text{m}$ ) as shown in Fig. 2(b - dashed box). The ROI is separated by 10  $\mu\text{m}$  from each pore wall, where one side is aligned with the pore inlet. The normalized intensity gray value  $\frac{I}{I_0}$ , where  $I_0$  is the initial intensity, of each pixel is measured along the pore, and plotted versus distance  $x$  along the pore (Fig. 2(c)). As fluorescein transports out of the pore,  $\frac{I}{I_0}$  decreases with time. A typical error of about 1.5% is observed for the intensity data ( $\frac{I}{I_0}$ ) with a maximum error of about 5% near the entrance of the pore.

## 3 Mathematical model

In this section, we discuss the details of our mathematical model. We consider a one-dimensional pore geometry of length  $\ell$ , as shown in Fig. 2(a). We assume that there are two electrolytes, A (cation concentration  $c_1$ , anion concentration  $c_2$ ) and B (cation concentration  $c_1$ , anion concentration  $c_3$ ), such that the cation of electrolytes A and B is common. The model allows for different valences of the cations and the anions. We assume that the pore is initially filled only with electrolyte A and that there is a fixed concentration of electrolyte B at the pore inlet ( $x = 0$ ). Lastly, we assume that the solution is electroneutral everywhere, the electric current is zero for all  $x$ , and the physical conditions are such that Nernst-Planck equations are valid; these are all standard assumptions for such chemically driven transport processes.

We denote the concentration of the cation as  $c_1(x, t)$  and the concentration of the anions as  $c_2(x, t)$  and  $c_3(x, t)$ , where  $t$  is time. The valence and diffusivities of the  $i^{\text{th}}$  ions are given as  $z_i$  (where  $z_i > 0$  for cations and  $z_i < 0$  for anions) and  $D_i$ , respectively. The species balance of the  $i^{\text{th}}$  ion is given by the Nernst-Planck equation<sup>1</sup>

$$\frac{\partial c_i}{\partial t} = -\frac{\partial J_i}{\partial x} = D_i \frac{\partial^2 c_i}{\partial x^2} + \frac{z_i e D_i}{k_B T} \frac{\partial}{\partial x} \left( c_i \frac{\partial \psi}{\partial x} \right), \quad (1)$$

where  $J_i$  is the flux of the  $i^{\text{th}}$  ion,  $\psi$  is the electric potential,  $e$  is the charge of an electron,  $k_B$  is the Boltzmann constant and  $T$  is the temperature. The electroneutrality condition ( $\sum z_i c_i = 0$ ) and a zero electric current condition ( $\sum_i z_i J_i = 0$ ) yields<sup>8,9,13,14,19,33</sup>

$$\frac{\partial \psi}{\partial x} = -\frac{k_B T}{e} \frac{\sum_i z_i D_i \frac{\partial c_i}{\partial x}}{\sum_i z_i^2 D_i c_i}. \quad (2)$$

This equation makes clear that the concentration of all of the ions influences the local electric field which in turn generates electromigration of ions (Eq. (1)). Furthermore, we note that the electric field vanishes when ion concentrations are spatially constant. We non-dimensionalize variables as  $X = \frac{x}{\ell}$ ,  $\Psi = \frac{e\psi}{k_B T}$ ,

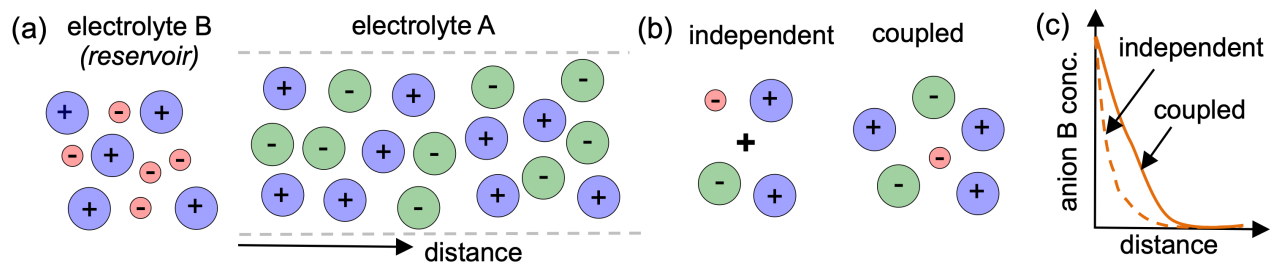


**Fig. 1 Effect of multiple electrolytes.** (a) Consider a setup where electrolyte A is brought in contact with a reservoir of electrolyte B. The cation of electrolytes A and B is common. (b) If transport of electrolytes A and B is independent, they need to satisfy electroneutrality separately. However, if we allow for the ionic fluxes to be coupled with each other, electroneutrality needs to be satisfied collectively. (c) If the diffusivity of anions of electrolyte B is much larger than all the remaining ions, the independent electrolyte analysis predicts a slower diffusion rate for the anion of electrolyte B as compared to the analysis where ionic fluxes are coupled.

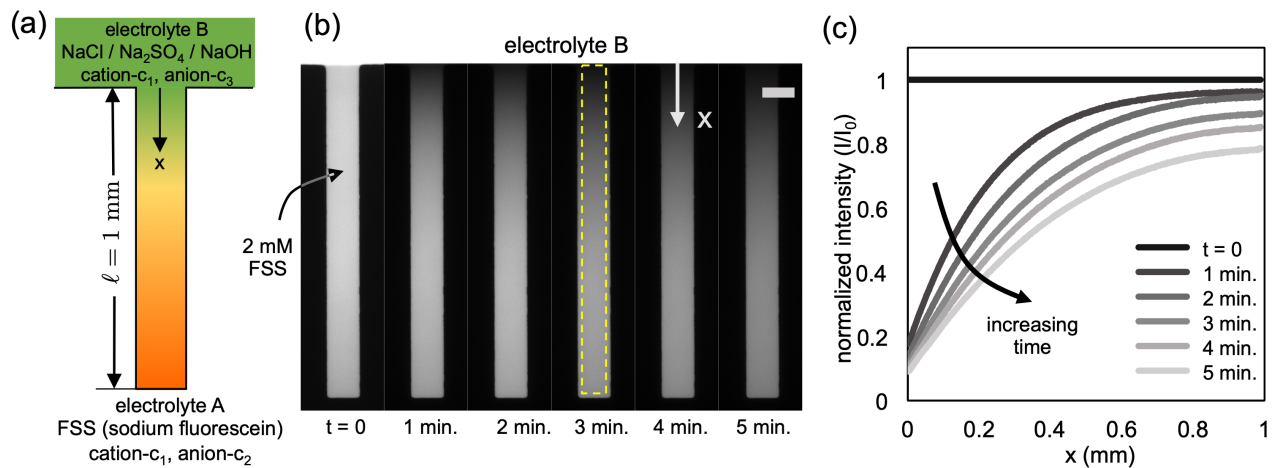


**Fig. 2 Multiple electrolyte diffusion experiments.** (a) The one-dimensional diffusion experiments are set up by using a dead-end pore geometry<sup>30,31</sup>, where the pores are initially filled with electrolyte A, here 2 mM sodium fluorescein salt (FSS). The main channel is flooded with electrolyte B, e.g., NaCl, Na<sub>2</sub>SO<sub>4</sub> and NaOH. The concentration and type of electrolyte B is varied to observe the effect on diffusion of fluorescein. (b) Time sequence of fluorescent images obtained from an experiment with a 2 mM FSS (electrolyte A) - 2 mM NaCl (electrolyte B) pair. Diffusion of ions is visualized by the concentration of fluorescein in the pore at different times. Dashed box ( $80 \mu\text{m} \times 990 \mu\text{m}$ ) is the region of interest (ROI) for the intensity analysis. Scale bar is  $100 \mu\text{m}$ . (c) Normalized gray values along the pore (or ROI) are plotted versus distance along the pore ( $x$ ) for different times, which yields the diffusion profile of fluorescein.

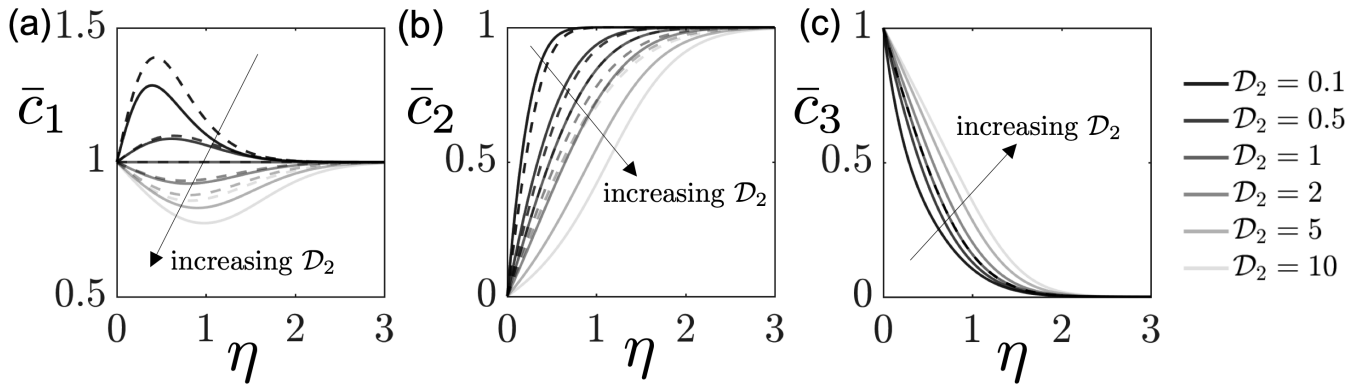


**Fig. 3 Overview of the semi-infinite model - effect of  $\mathcal{D}_2$ .** (a)  $\bar{c}_1(\eta)$ , (b)  $\bar{c}_2(\eta)$  and (c)  $\bar{c}_3(\eta)$  for the fully coupled analysis (Eq. (4)) as well as for the independent electrolyte analysis (Eq. (5)). Results are presented for fixed  $z_1 = -z_2 = -z_3 = \mathcal{D}_1 = \mathcal{D}_3 = \beta = 1$ , and varying  $\mathcal{D}_2$ . The solid and dashed lines are predictions from Eqs. (4) and (5) respectively. In (c), the prediction of Eq. (5), *i.e.*,  $\bar{c}_3 = \text{erfc}(\eta)$ , overlaps for all different  $\mathcal{D}_2$  with the prediction of Eq. (4) for  $\mathcal{D}_2 = 1$ .

$\tau = \frac{tD^*}{l^2}$  and  $\mathcal{D}_i = \frac{D_i}{D^*}$ , where  $D^*$  is a characteristic diffusivity. Thus we obtain the coupled partial differential equations ( $i = 1, 2, 3$ )<sup>8,9,13,14</sup>

$$\frac{\partial c_i}{\partial \tau} = \mathcal{D}_i \frac{\partial^2 c_i}{\partial X^2} - z_i \mathcal{D}_i \frac{\partial}{\partial X} \left( c_i \frac{\sum_j z_j \mathcal{D}_j \frac{\partial c_j}{\partial X}}{\sum_j z_j^2 \mathcal{D}_j c_j} \right). \quad (3)$$

Eq. (3) shows that for a multi-ion system space, the flux of the  $i^{\text{th}}$  ion is coupled to every other ion. We describe the initial and boundary conditions in Sections 3.1 and 3.2.

We note that electroneutrality is implicit in Eq. (3). For electroneutrality to be valid, we need to specify an initial condition that satisfies electroneutrality. There is also an alternative route where we can utilize electroneutrality explicitly. In this approach, we can eliminate one ion concentration, say  $c_3$ , using electroneutrality and solve for the remaining ion concentrations, *i.e.*,  $c_1$  and  $c_2$ . Next,  $c_3$  can be recovered by using  $\sum z_i c_i = 0$ . These approaches are equivalent but we utilize the implicit approach since it enables us to express Eq. (3) in a compact form.

### 3.1 Semi-infinite analysis

We consider the semi-infinite scenario of a long pore such that  $0 \leq X \leq \infty$ . Here, the concentration are appropriately scaled so that initial conditions are  $c_1(X, 0) = 1$ ,  $c_2(X, 0) = \left| \frac{z_1}{z_2} \right|$  and  $c_3(X, 0) = 0$ . The boundary conditions at the pore inlet are  $c_1(0, \tau) = \beta$ ,  $c_2(0, \tau) = 0$  and  $c_3(0, \tau) = \left| \frac{z_1}{z_3} \right| \beta$ , where  $\beta$  indicates the relative concentration between the reservoir and the pore. The boundary conditions for large  $X$  are  $c_1(\infty, \tau) = 1$ ,  $c_2(\infty, \tau) = \left| \frac{z_1}{z_2} \right|$  and  $c_3(\infty, \tau) = 0$ . To solve Eq. (3) for the semi-infinite domain, we introduce a similarity variable  $\eta = \frac{X}{\sqrt{4\tau}}$  such that  $c_i(X, \tau) = \bar{c}_i(\eta)$ . Therefore, Eq. (3) reduces to ( $i = 1, 2, 3$ )

$$2\eta \frac{d\bar{c}_i}{d\eta} + \mathcal{D}_i \frac{d^2 \bar{c}_i}{d\eta^2} - z_i \mathcal{D}_i \frac{d}{d\eta} \left( \bar{c}_i \frac{\sum_j z_j \mathcal{D}_j \frac{d\bar{c}_j}{d\eta}}{\sum_j z_j^2 \mathcal{D}_j \bar{c}_j} \right) = 0, \quad (4)$$

where  $\bar{c}_1(0) = \beta$ ,  $\bar{c}_2(0) = 0$ ,  $\bar{c}_3(0) = \left| \frac{z_1}{z_3} \right| \beta$ , and  $\bar{c}_1(\infty) = 1$ ,  $\bar{c}_2(\infty) = \left| \frac{z_1}{z_2} \right|$ ,  $\bar{c}_3(\infty) = 0$ .

We solve Eq. (4) numerically by using the finite-difference method. We note that dimensionless parameters that dictate the solution of Eq. (4) are  $z_i$ ,  $\mathcal{D}_i$  and  $\beta$ . In experiments,  $\mathcal{D}_i$  and  $z_i$  can be varied by changing the electrolyte, and the parameter  $\beta$  can be varied by changing the concentration of the electrolytes.

We compare the predictions of Eq. (4) with the scenario where electrolytes A and B do not influence their respective fluxes, and the concentration of ions are calculated based on standard results, *i.e.*, each ion pair satisfies a separate one-dimensional diffusion equation with an ambipolar diffusion constant<sup>1,3,22</sup>

$$\bar{c}_1 = \text{erf} \left( \frac{\eta}{\sqrt{\mathcal{D}_a^{12}}} \right) + \beta \text{erfc} \left( \frac{\eta}{\sqrt{\mathcal{D}_a^{13}}} \right), \quad (5a)$$

$$\bar{c}_2 = \left| \frac{z_1}{z_2} \right| \text{erf} \left( \frac{\eta}{\sqrt{\mathcal{D}_a^{12}}} \right), \quad (5b)$$

$$\bar{c}_3 = \left| \frac{z_1}{z_3} \right| \beta \text{erfc} \left( \frac{\eta}{\sqrt{\mathcal{D}_a^{13}}} \right), \quad (5c)$$

where  $\mathcal{D}_a^{12} = \frac{(z_1 - z_2) \mathcal{D}_1 \mathcal{D}_2}{z_1 \mathcal{D}_1 - z_2 \mathcal{D}_2}$  and  $\mathcal{D}_a^{13} = \frac{(z_1 - z_3) \mathcal{D}_1 \mathcal{D}_3}{z_1 \mathcal{D}_1 - z_3 \mathcal{D}_3}$  are ambipolar diffusivities of electrolytes A and B.

We analyse the scenario where  $z_1 = -z_2 = -z_3 = \mathcal{D}_1 = \mathcal{D}_3 = \beta = 1$ , and  $\mathcal{D}_2$  varies. The predictions for Eqs. (4) and (5) are summarized in Fig. 3. As evident from the results, Eq. (4) (solid lines) yields different predictions than Eq. (5) (dashed lines). We note some of the trends observed in Fig. 3:

- (i)  $\bar{c}_1(\eta)$  from Eq. (4) overlaps with Eq. (5) when  $\mathcal{D}_2 = 1$  as  $\frac{\partial \Psi}{\partial X} = 0$ ; see Eq. (2), *i.e.*, such conditions are purely diffusive with no electromigration contributions.
- (ii)  $\bar{c}_1(\eta)$  has a maximum for  $\mathcal{D}_2 < 1$ , where the maximum value is smaller for Eq. (4) than Eq. (5). In contrast,  $\bar{c}_1(\eta)$  has a minimum for  $\mathcal{D}_2 > 1$ , where the minimum value is smaller for Eq. (4) than Eq. (5).

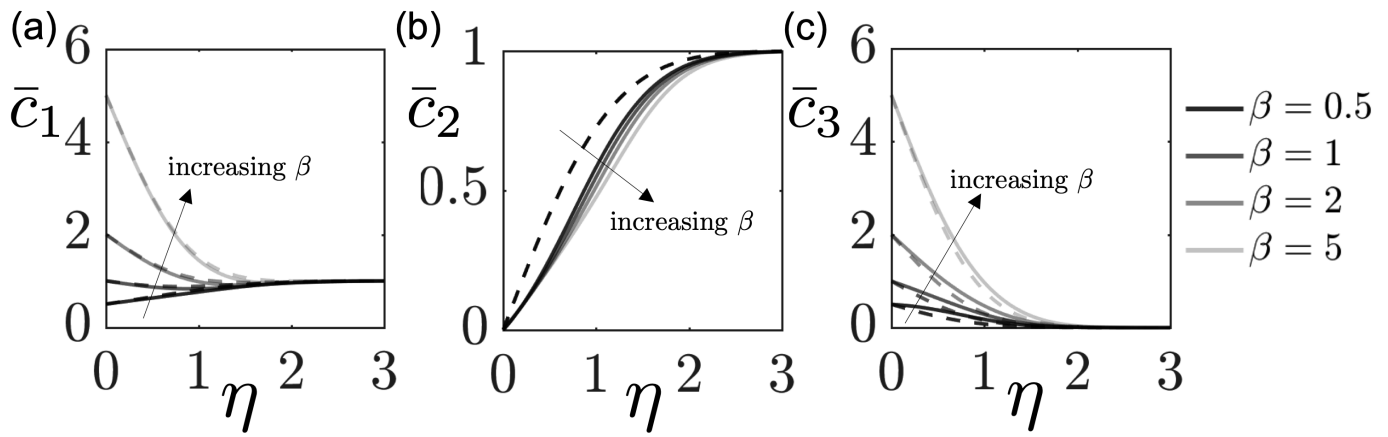


**Fig. 4 Overview of the semi-infinite model - effect of  $\beta$ .** (a)  $\bar{c}_1(\eta)$ , (b)  $\bar{c}_2(\eta)$  and (c)  $\bar{c}_3(\eta)$ , for the fully coupled analysis (Eq. (4)) as well as for the independent electrolyte analysis (Eq. (5)). Results are presented for fixed  $z_1 = -z_2 = -z_3 = \mathcal{D}_1 = \mathcal{D}_3 = 1$  and  $\mathcal{D}_2 = 5$ , and varying  $\beta$ . The solid and dashed lines are predictions from Eqs. (4) and (5) respectively. In (b), the predictions of  $\bar{c}_2$  from Eq. (5), *i.e.*, the dashed lines overlap for different values of  $\beta$ .

- (iii) For  $\mathcal{D}_2 < 1$ ,  $\bar{c}_2(\eta)$  diffuses out of the pore slower for Eq. (4) than Eq. (5). The opposite is true for  $\mathcal{D}_2 > 1$ , *i.e.*,  $\bar{c}_2(\eta)$  diffuses out of the pore faster for Eq. (4) than Eq. (5).
- (iv) For  $\mathcal{D}_2 < 1$ ,  $\bar{c}_3(\eta)$  diffuses into the pore slower for Eq. (4) than Eq. (5). The opposite is true for  $\mathcal{D}_2 > 1$ , *i.e.*,  $\bar{c}_3(\eta)$  diffuses into the pore faster for Eq. (4) than Eq. (5).

To understand these trends, we consider the limiting cases of  $\mathcal{D}_2 \ll 1$  and  $\mathcal{D}_2 \gg 1$ . We recall that the pore is initially filled with  $\bar{c}_1$  and  $\bar{c}_2$ , and the reservoir consists of  $\bar{c}_1$  and  $\bar{c}_3$ . Moreover, for the conditions reported in Fig. 3, the concentration of the cation in the reservoir is equal to the initial concentration of cation in the pore ( $\beta = 1$ ).

We first discuss the physical interpretation of the independent electrolyte analysis for the limiting case of  $\mathcal{D}_2 \ll 1$ . Since  $\bar{c}_1$  and  $\bar{c}_2$  inside the pore do not interact with the ions in the reservoir, both the ions prefer to diffuse out of the pore. For  $\mathcal{D}_2 \ll 1$ ,  $c_1$  slows down to satisfy electroneutrality with  $\bar{c}_2$ . To enable this, an electric field develops such that  $\frac{\partial \Psi}{\partial X} > 0$ . This electric field retards and promotes the diffusion of  $\bar{c}_1$  and  $\bar{c}_2$  out of the pore, respectively. In addition, since the  $\bar{c}_1$  in the reservoir does not interact with the  $\bar{c}_1$  ions inside the pore, the cations from the reservoir diffuse inside the pore, creating a maximum in  $\bar{c}_1$ ; see Fig. 3(a), dashed lines. Therefore, the smaller the value of  $\mathcal{D}_2$ , the larger the maximum value of  $\bar{c}_1$ . Similarly, we learn that the smaller the value of  $\mathcal{D}_2$ , the slower is the diffusion of  $\bar{c}_2$  out of the pore; see Fig. 3(b), dashed lines. Lastly,  $\bar{c}_3$  simply diffuses inside the pore and changes in the value of  $\mathcal{D}_2$  do not affect  $\bar{c}_3$ ; see Fig. 3(c) dashed lines; also see Eq. (5).

We now compare and contrast the above discussion with the physical interpretation of the electrokinetically consistent coupled analysis for the limiting case of  $\mathcal{D}_2 \ll 1$ . Since all of the ions interact with each other, initially there is no concentration gradient of  $\bar{c}_1$ . Therefore, the electric field that develops to satisfy electroneutrality is weaker as compared to the independent analysis case. In addition, the gradient experienced by  $\bar{c}_1$  in the reservoir is also smaller, and therefore, the maxima of  $\bar{c}_1(\eta)$

is smaller in magnitude; see Fig. 3(a), solid lines. Since the electric field is weaker,  $\bar{c}_2$  diffuses out of the pore slower than the independent electrolyte analysis; Fig. 3(b), solid lines. Lastly, since the overall accumulation of the cations inside the pore is smaller, the diffusion of  $\bar{c}_3$  inside the pore is slower to satisfy electroneutrality; see Fig. 3(c), solid lines. We note that the effect of  $\mathcal{D}_2$  on  $\bar{c}_3$  is crucial since it highlights the coupled nature of the multi-electrolyte systems.

Next, we briefly summarize the physical interpretation of the limiting case of  $\mathcal{D}_2 \gg 1$ . For  $\mathcal{D}_2 \gg 1$ , the independent analysis for  $\bar{c}_1$  and  $\bar{c}_2$  is controlled by the ambipolar diffusivity. Therefore, in this limit, the concentrations become independent of  $\mathcal{D}_2$  as the ambipolar diffusivity approaches  $\mathcal{D}_1$ . Indeed, this response is observed for all  $\bar{c}_i$  in our numerical calculations; see Fig. 3, dashed lines. In this scenario, since the electric field will develop to retard the motion of  $\bar{c}_2$  out of the pore,  $\frac{\partial \Psi}{\partial X} < 0$ . Therefore,  $\bar{c}_1(\eta)$  shows a minimum, which starts to become independent of  $\mathcal{D}_2$  for larger values of  $\mathcal{D}_2$ ; see Fig. 3(a), dashed lines. Similarly, diffusion of  $\bar{c}_2$  and  $\bar{c}_3$  approaches a limiting value for larger values of  $\mathcal{D}_2$ ; see Fig. 3(b),(c), dashed lines. In contrast, for the coupled analysis, the transport of  $\bar{c}_i$  out of and into the pore is not limited by the ambipolar diffusivities of  $\bar{c}_1$  and  $\bar{c}_2$  because the ions have to satisfy the electroneutrality condition collectively, and not individually. Therefore, the electric field is stronger for the coupled analysis and  $\bar{c}_1$  shows a smaller value for the minima; Fig. 3(a), solid lines. In addition,  $\bar{c}_2$  and  $\bar{c}_3$  diffuse out of and into the pore faster as compared to the independent analysis; see Fig. 3(b),(c), solid lines.

We emphasize that the diffusivity contrast is an effective way to tune the transport of multi-electrolyte systems. For instance, in microfluidic studies, if acids and bases are used as electrolytes<sup>25</sup>, the diffusivity contrast due to large diffusivities of  $H^+$  and  $OH^-$  ions enables a useful tool to manipulate colloidal transport<sup>19,26</sup>. In fact, we provide experimental evidence for the same by using  $OH^-$  as the anion in the reservoir; see Section 4.

We now summarize the effect of  $\beta$  when  $z_1 = -z_2 = -z_3 =$

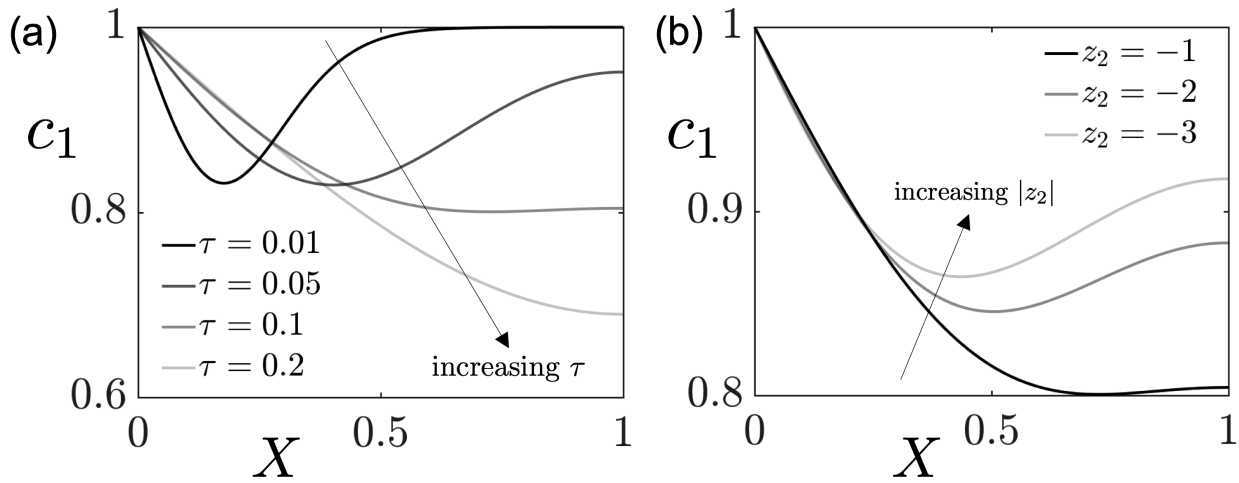


**Fig. 5 Overview of the finite pore analysis.** (a)  $c_1(X, \tau)$  for different  $\tau$  with fixed  $z_1 = -z_2 = -z_3 = \mathcal{D}_1 = \mathcal{D}_3 = \beta = 1$  and  $\mathcal{D}_2 = 5$ , and (b)  $c_1(X, \tau)$  for different  $z_2$  with fixed  $z_1 = -z_3 = \mathcal{D}_1 = \mathcal{D}_3 = \beta = 1$ ,  $\tau = 0.1$  and  $\mathcal{D}_2 = 5$ . The solid lines are predictions for the coupled electrolyte model (Eq. (3)).

$\mathcal{D}_1 = \mathcal{D}_3 = 1$  and  $\mathcal{D}_2 = 5$ ; see Fig. 4. Our results indicate that the independent and coupled analyses predict a relatively similar profile for  $\bar{c}_1$  and  $\bar{c}_3$ ; see Fig. 4(a), (c). However, the profile for  $\bar{c}_2$ , the anion initially in the pore, varies significantly between the two models; Fig. 4(b). The effect of reservoir concentration  $\beta$  is not observed in the independent (linear) model because the electrolytes do not interact with each other. Therefore, any change in concentration of the electrolyte in the reservoir does not change the behavior of  $\bar{c}_2$ . In contrast, for the coupled model, for  $\beta \gg 1$ ,  $\bar{c}_2$  can diffuse out more easily since it is not restricted to satisfy electroneutrality separately.

We highlight that the changes in  $\beta$  are readily performed in experiments by changing the concentration of the electrolyte in the main channel; see Fig. 2. In Section 4, we provide experimental evidence for the dependence of  $\bar{c}_2$  on  $\beta$ .

### 3.2 Finite pore analysis

In this section, we discuss the effect of the finite pore length. We solve Eq. (3) numerically using the method of lines<sup>34</sup> with the following initial and boundary conditions:  $c_1(X, 0) = 1$ ,  $c_2(X, 0) = \left| \frac{z_1}{z_2} \right|$ ,  $c_3(X, 0) = 0$ ,  $c_1(0, \tau) = \beta$ ,  $c_2(0, \tau) = 0$ ,  $c_3(0, \tau) = \left| \frac{z_1}{z_3} \right| \beta$ ,  $\left. \frac{\partial c_1}{\partial X} \right|_{X=1} = 0$ ,  $\left. \frac{\partial c_2}{\partial X} \right|_{X=1} = 0$  and  $\left. \frac{\partial c_3}{\partial X} \right|_{X=1} = 0$ . The results are summarized in Fig. 5.

We discuss the scenario of  $z_1 = -z_2 = -z_3 = \mathcal{D}_1 = \mathcal{D}_3 = \beta = 1$  and  $\mathcal{D}_2 = 5$ . As discussed previously, for  $\mathcal{D}_2 > 1$ ,  $\frac{\partial \Psi}{\partial X} < 0$ , and cations diffuse out of the pore. Therefore, for early times, *i.e.*,  $\tau \ll 1$ , we observe a minimum for  $c_1(X, \tau)$ , similar to the semi-infinite analysis; see Fig. 5(a). For longer times, the finite-pore length effects start to become important and we no longer observe a minimum for  $c_1$  versus  $X$ . Instead, the concentration monotonically decreases with  $X$ . Therefore, for predicting long time behavior of an experiment, it is crucial to include the finite-pore length effect.

We also investigate the effect of different  $z_2$  for fixed  $z_1 = -z_3 = D_1 = D_3 = \beta = 1$ ,  $D_2 = 5$  and  $\tau = 0.1$ . We recall that  $\frac{\partial \Psi}{\partial X} = -\frac{\sum z_i \mathcal{D}_i \frac{\partial c_i}{\partial X}}{\sum z_i^2 \mathcal{D}_i c_i}$

(Eq. (2)). Therefore, for a larger  $|z_2|$ ,  $\left| \frac{\partial \Psi}{\partial X} \right|$  is smaller, and the minimum value of  $c_1$  decreases with an increase in  $|z_2|$ ; see Fig. 5(b).

We have provided modeling details for the semi-infinite coupled analysis (Eq. (4)), the semi-infinite independent analysis (Eq. (5)), and the finite pore coupled analysis (Eq. (3)). For completeness, we also provide the finite pore independent analysis. In the independent analysis, each ion pair satisfies a separate one-dimensional diffusion equation with an ambipolar diffusion constant. For a finite length domain, the concentrations are calculated through a series solution<sup>1</sup>

$$c_2(X, \tau) = \left| \frac{z_1}{z_2} \right| \sum_{k=0}^{\infty} \frac{2}{\lambda_k} \sin(\lambda_k X) \exp\left(-\lambda_k^2 \mathcal{D}_a^{12} \tau\right), \quad (6a)$$

$$c_3(X, \tau) = \left| \frac{z_1}{z_3} \right| \beta \left( 1 - \sum_{k=0}^{\infty} \frac{2}{\lambda_k} \sin(\lambda_k X) \exp\left(-\lambda_k^2 \mathcal{D}_a^{13} \tau\right) \right), \quad (6b)$$

where  $\lambda_k = (2k+1)\frac{\pi}{2}$ ,  $\mathcal{D}_a^{12} = \frac{(z_1 - z_2)\mathcal{D}_1\mathcal{D}_2}{z_1\mathcal{D}_1 - z_2\mathcal{D}_2}$  and  $\mathcal{D}_a^{13} = \frac{(z_1 - z_3)\mathcal{D}_1\mathcal{D}_3}{z_1\mathcal{D}_1 - z_3\mathcal{D}_3}$  are ambipolar diffusivities of electrolytes A and B. The value of  $c_1$  can be calculated as  $c_1 = \left| \frac{z_2}{z_1} \right| c_2 + \left| \frac{z_3}{z_1} \right| c_3$ .

## 4 Comparison of results from experiments and model

In this section, we compare the results of our experiments with the mathematical model described in the previous section. As described in Section 2, the common cation between the pore and the reservoir in our setup is  $\text{Na}^+$ . The anion initially filled in the pore is (fluorescein)  $\text{Fl}^{2-}$ , and the anion in the main channel (reservoir) is either  $\text{Cl}^-$ ,  $\text{SO}_4^{2-}$ , or  $\text{OH}^-$ . Therefore,  $z_1 = 1$ ,  $z_2 = -2$  and  $z_3 = -1$ ,  $z_3 = -2$ , or  $z_3 = -1$ . Assuming  $D^* = D_{\text{Fl}}$ ,  $\mathcal{D}_1 = \frac{D_{\text{Na}}}{D_{\text{Fl}}}$ ,  $\mathcal{D}_2 = 1$  and  $\mathcal{D}_3 = \left[ \frac{D_{\text{Cl}}}{D_{\text{Fl}}}, \frac{D_{\text{SO}_4}}{D_{\text{Fl}}}, \frac{D_{\text{OH}}}{D_{\text{Fl}}} \right]$ . Based on values of diffusivities reported in literature,  $\mathcal{D}_1 = 2.1$  and  $\mathcal{D}_3 = [3.1, 1.6, 8.2]$ .<sup>28,35</sup>

Since the experimental running time is 5 min, the upper limit for the dimensionless time is  $\tau = \frac{tD^*}{L^2} \approx 0.2$ . Therefore, finite-pore effects could become important and we numerically solve Eq. (3)

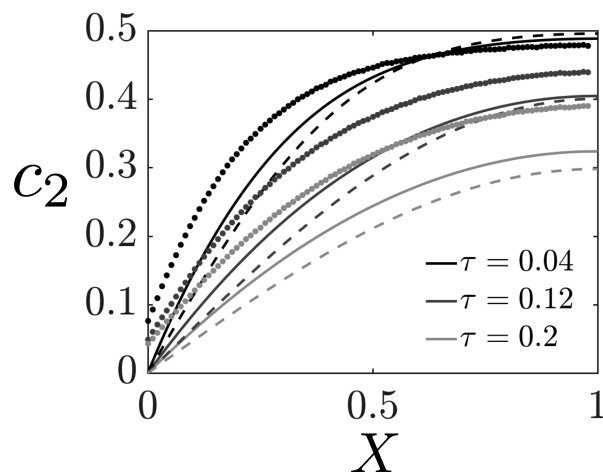


**Fig. 6 Comparison between experiments, the coupled electrolyte model, and the independent electrolyte model - effect of  $\tau$ .** Fluorescein concentration  $c_2(X, \tau)$  for  $\beta = 1$ , where  $\beta = 1$  corresponds to the concentration of 4 mM NaCl in the main channel (Fig. 2). The solid lines are results for the coupled electrolyte model (Eq. (3)), the dashed lines are results for the independent electrolyte model (Eq. (6)), and the data points are obtained from experiments.

to simulate the concentration profiles. The initial and boundary conditions employed are  $c_1(X, 0) = 1$ ,  $c_2(X, 0) = 0.5$ ,  $c_3(X, 0) = 0$ ,  $c_1(0, \tau) = \beta$ ,  $c_2(0, \tau) = 0$ ,  $c_3(0, \tau) = \frac{z_1}{z_3} \beta$ ,  $\frac{\partial c_1}{\partial X} \Big|_{X=1} = 0$ ,  $\frac{\partial c_2}{\partial X} \Big|_{X=1} = 0$  and  $\frac{\partial c_3}{\partial X} \Big|_{X=1} = 0$ . Eq. (6) is used to calculate the concentration profiles for the independent electrolyte model. The overview of the comparison between experiments and the models is provided in Figs. 6 and 7.

First, we focus on the scenario when NaCl is flooded in the main channel with a concentration of 4 mM ( $\beta = 1$ ). Since the fluorescein is transported out of the pore,  $c_2$  decreases with an increase in  $\tau$ . Our experiments and model display a qualitative and a reasonable quantitative agreement; see Fig. 6. We emphasize that the coupled model is able to reproduce the experimental trends without any fitting parameters. In addition, we find that the coupled model displays better agreement than the independent electrolyte model.

Second, we focus on the effect of  $\beta$  with NaCl as the electrolyte in the reservoir. Since the fluorescein ion is transported out of the pore, as evident from Fig. 4(b),  $c_2$  is sensitive to the value of  $\beta$ . We recall that for experimental conditions  $\mathcal{D}_1 = 2.1$ ,  $\mathcal{D}_2 = 1$  and  $\mathcal{D}_3 = 3.1$ . Based on Eq. (2), with an increase in the value of  $\beta$ ,  $\frac{\partial \Psi}{\partial X}$  becomes more negative. Therefore, the rate at which  $c_2$  is transported out of the pore is slower with an increase in the value of  $\beta$ . This trend is observed for both experiments and the coupled electrolyte model; see Fig. 7(a). However, the independent electrolyte model does not show any dependence on  $\beta$ .

Lastly, we detail the effect of varying ion diffusivities by changing the electrolyte in the reservoir; see Fig. 7(b). We fixed the electrolyte concentrations in the reservoir such that  $\beta = 1$  for all the different electrolytes, *i.e.*, we utilized 4 mM NaCl, 2 mM Na<sub>2</sub>SO<sub>4</sub> and 4 mM NaOH. The diffusivities for NaCl, Na<sub>2</sub>SO<sub>4</sub> and NaOH are  $\mathcal{D}_3 = 3.1$ ,  $\mathcal{D}_3 = 1.6$  and  $\mathcal{D}_3 = 8.2$ ,

respectively. Physically, we know that when  $\mathcal{D}_3$  is large, it is easier for fluorescein to transport out of the pore as there is less restriction for fluorescein to remain inside the pore to satisfy electroneutrality. Therefore, we observe that when Na<sub>2</sub>SO<sub>4</sub> is the reservoir electrolyte, fluorescein diffuses out the slowest, and when NaOH is the reservoir electrolyte, fluorescein diffuses out the fastest (Fig. 7(b)). We observe the above trend for both experiments and the coupled electrolyte model. In contrast, the independent electrolyte model predicts the same transport rate for the fluorescein ion irrespective of the reservoir electrolyte. The results in Fig. 7 underscore the importance of the coupled electrolyte model.

There are some quantitative differences between the model predictions and the experimental data, especially because the boundary condition utilized in the model at  $X = 0$  is not strictly observed in experiments; see Figs. 6 and 7. Based on our experimental data,  $c_2(0, \tau) \approx 0.06$  is approximately followed. Therefore, we perform the finite-pore simulations (Eq. 3) by appropriately modifying the boundary conditions, and obtain better agreement between the coupled model and the experiments (see Supporting Information). To further improve upon our predictions, two-dimensional and three-dimensional models are required. In these models, Eq. (3) is modified to also include the diffusioosmotic transport of ions. Shin et al.<sup>36</sup> performed a similar analysis for a single electrolyte and demonstrated that the multi-dimensional models predict a slower transport rate of ions as compared to the corresponding one-dimensional model. Indeed, we observe that the one-dimensional model systematically over predicts the transport of the fluorescein ion (Figs. 6 and 7). Therefore, to accurately capture the details of the ion transport inside the pore, a multi-dimensional model for multiple electrolytes is required and will be pursued in our future studies. Nonetheless, we emphasize that the model is able to capture the experimental trends for the influence of multiple ions without any fitting parameters, and provides useful insights into the behaviour of diffusion in multiple electrolytes.

## 5 Conclusion

In this article, we investigated the diffusion of ions in a system with two binary electrolytes as a means for understanding the influence of background ions. We developed a mathematical model to predict the ion concentration profiles in a one-dimensional semi-infinite geometry as well as a finite-sized geometry. Our theoretical predictions demonstrate that it is crucial to consider the coupling between ionic fluxes to accurately predict the diffusive transport of ions (both the time scale and the magnitude of concentration variations). We find that our theoretical predictions based on the Nernst-Planck description of ionic transport are in good agreement with our experimental data. We also note that the independent electrolyte analysis is unable to capture some of the details, especially when the concentration and diffusivity ratios are large.

A direct application of our work is the experimental determination of an ion diffusion coefficient by utilizing multiple electrolytes so as to reduce the effect of traces of unwanted



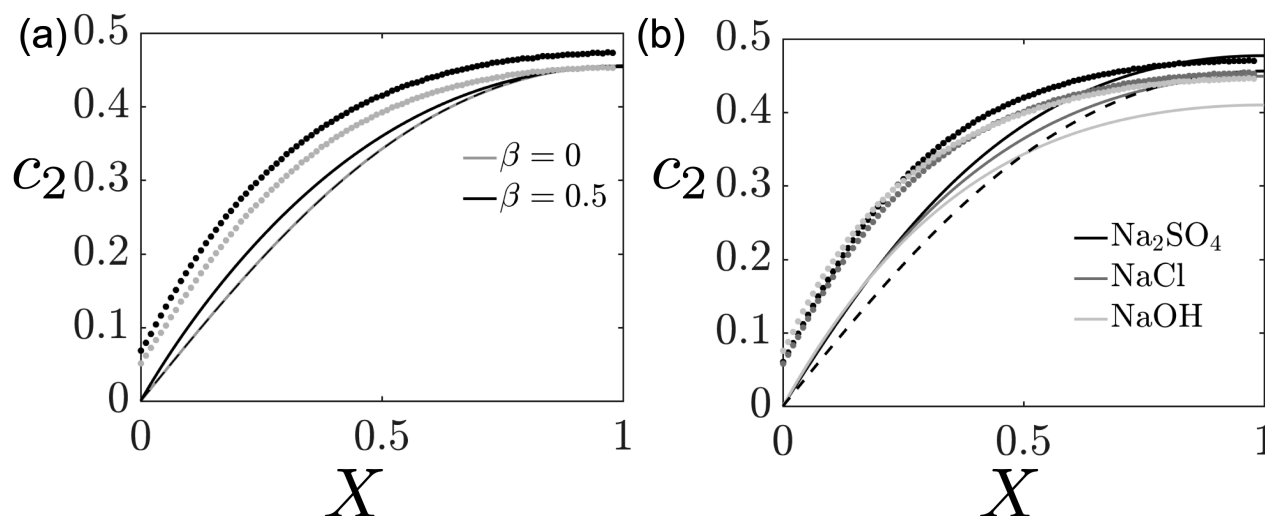


**Fig. 7 Comparison between experiments, the coupled electrolyte model and the independent electrolyte model - effect of  $\beta$  and different reservoir electrolytes.** (a) Fluorescein concentration  $c_2(X, \tau)$  for different  $\beta$ ,  $\tau = 0.08$  and NaCl as the reservoir electrolyte.  $\beta = 0$  and  $\beta = 0.5$  implies NaCl concentrations in the main channel are 0 mM and 2 mM respectively. The dashed lines overlap for different  $\beta$ . (b) Fluorescein concentration  $c_2(X, \tau)$  for  $\beta = 1$ ,  $\tau = 0.08$  and different reservoir electrolytes.  $\beta = 1$  implies NaCl, Na<sub>2</sub>SO<sub>4</sub> and NaOH concentrations in the main channel are 4 mM, 2 mM and 4 mM, respectively. The dashed lines overlap for different electrolytes. The solid lines are results for the coupled electrolyte model (Eq. (3)), the dashed lines are results for the independent electrolyte model (Eq. (6)), and the data points are obtained from experiments.

ions. Looking forward, the key parameters that can be exploited to tune the motion of ions, and by extension the motion of colloids,<sup>22,25,26</sup> are the relative diffusivities and concentration of ions. These ratios dictate the direction and strength of the electric field, which influences the diffusion of ions. Therefore, multiple electrolytes can be exploited for electrokinetic processes such as electrophoresis and diffusiophoresis. Our results can also be extended to systems with a finite current such as supercapacitors<sup>27,37</sup> and capacitive deionization<sup>38</sup>, where solutions often contain multiple electrolytes, as well as materials (concrete) systems<sup>6–10</sup> and environmental (soil) applications.<sup>39–42</sup>

## Conflicts of interest

There are no conflicts to declare.

## Acknowledgements

We thank the Andlinger Center for Energy and the Environment at Princeton University and the NSF grant CBET-1702693 for financial support for our research.

## References

- W. M. Deen, *Analysis of Transport Phenomena*, Oxford University Press New York, 2012.
- E. L. Cussler, *Multicomponent Diffusion*, Elsevier, 2013.
- R. B. Bird, W. E. Stewart and E. N. Lightfoot, *Transport Phenomena*, John Wiley & Sons, 2006.
- J. Newman and K. E. Thomas-Alyea, *Electrochemical Systems*, John Wiley & Sons, 2012.
- A. Persat and J. G. Santiago, *Current Opinion in Colloid & Interface Science*, 2016, **24**, 52–63.
- Y. Hosokawa, K. Yamada, B. Johannesson and L.-O. Nilsson, *Materials and Structures*, 2011, **44**, 1577–1592.
- B. Johannesson, K. Yamada, L.-O. Nilsson and Y. Hosokawa, *Materials and Structures*, 2007, **40**, 651.
- O. Truc, J.-P. Ollivier and L.-O. Nilsson, *Materials and Structures*, 2000, **33**, 566–573.
- O. Truc, J.-P. Ollivier and L.-O. Nilsson, *Cement and Concrete Research*, 2000, **30**, 1581–1592.
- Y. Bu, D. Luo and J. Weiss, *Advances in Civil Engineering Materials*, 2014, **3**, 566–585.
- G. Engelhardt and H.-H. Strehblow, *Journal of Electroanalytical Chemistry*, 1995, **394**, 7–15.
- D. Barba, G. Del Re and P. U. Foscolo, *The Chemical Engineering Journal*, 1983, **26**, 33–39.
- T. Tsuru, S. Nakao and S. Kimura, *Journal of Chemical Engineering of Japan*, 1991, **24**, 511–517.
- T. Tsuru, M. Urairi, S. Nakao and S. Kimura, *Journal of Chemical Engineering of Japan*, 1991, **24**, 518–524.
- D. G. Leaist and L. Hao, *Journal of the Chemical Society, Faraday Transactions*, 1993, **89**, 2775–2782.
- C. Liu, J. Shang and J. M. Zachara, *Water Resources Research*, 2011, **47**,.
- G. Narsilio, R. Li, P. Pivonka and D. Smith, *Cement and Concrete Research*, 2007, **37**, 1152–1163.
- S. S. Bahga, R. Moza and M. Khichar, *Proceedings of the Royal Society A: Mathematical, Physical and Engineering Sciences*, 2016, **472**, 20150661.
- T.-Y. Chiang and D. Velegol, *Journal of Colloid and Interface science*, 2014, **424**, 120–123.
- A. Donev, A. L. Garcia, J.-P. Péraud, A. Nonaka and J. B. Bell, *Current Opinion in Electrochemistry*, 2018, 1–10.
- A. Donev, A. J. Nonaka, C. Kim, A. L. Garcia and J. B. Bell, *Physical Review Fluids*, 2019, **4**, 043701.

- 22 D. Florea, S. Musa, J. M. Huyghe and H. M. Wyss, *Proceedings of the National Academy of Sciences*, 2014, **111**, 6554–6559.
- 23 M. H. Oddy and J. G. Santiago, *Physics of Fluids*, 2005, **17**, 064108.
- 24 J. S. Paustian, C. D. Angulo, R. Nery-Azevedo, N. Shi, A. I. Abdel-Fattah and T. M. Squires, *Langmuir*, 2015, **31**, 4402–4410.
- 25 N. Shi, R. Nery-Azevedo, A. I. Abdel-Fattah and T. M. Squires, *Physical Review Letters*, 2016, **117**, 258001.
- 26 A. Gupta, B. Rallabandi and H. A. Stone, *Physical Review Fluids*, 2019, **4**, 043702.
- 27 A. Gupta and H. A. Stone, *Langmuir*, 2018, **34**, 11971–11985.
- 28 D. Velegol, A. Garg, R. Guha, A. Kar and M. Kumar, *Soft Matter*, 2016, **12**, 4686–4703.
- 29 P. B. Warren, S. Shin and H. A. Stone, *Soft Matter*, 2019, **15**, 278–288.
- 30 A. Kar, T.-Y. Chiang, I. Ortiz Rivera, A. Sen and D. Velegol, *ACS nano*, 2015, **9**, 746–753.
- 31 S. Shin, E. Um, B. Sabass, J. T. Ault, M. Rahimi, P. B. Warren and H. A. Stone, *Proceedings of the National Academy of Sciences*, 2016, **113**, 257–261.
- 32 L. Song, E. Hennink, I. T. Young and H. J. Tanke, *Biophysical Journal*, 1995, **68**, 2588–2600.
- 33 A. Brown and W. Poon, *Soft Matter*, 2014, **10**, 4016–4027.
- 34 W. E. Schiesser, *The Numerical Method of Lines: Integration of Partial Differential Equations*, Elsevier, 2012.
- 35 P. Galambos and F. K. Forster, *Micro Total Analysis Systems* 98, 1998, pp. 189–192.
- 36 S. Shin, J. T. Ault, J. Feng, P. B. Warren and H. A. Stone, *Advanced Materials*, 2017, **29**, 1701516.
- 37 M. Z. Bazant, K. Thornton and A. Ajdari, *Physical Review E*, 2004, **70**, 021506.
- 38 P. Biesheuvel and M. Bazant, *Physical Review E*, 2010, **81**, 031502.
- 39 J. Virkutyte, M. Sillanpää and P. Latostenmaa, *Science of the Total Environment*, 2002, **289**, 97–121.
- 40 A. Ribeiro, J. Rodriguez-Maroto, E. Mateus and H. Gomes, *Chemosphere*, 2005, **59**, 1229–1239.
- 41 A. Z. Al-Hamdan and K. R. Reddy, *Journal of Geotechnical and Geoenvironmental Engineering*, 2008, **134**, 91–105.
- 42 A. P. Shapiro and R. F. Probstein, *Environmental Science & Technology*, 1993, **27**, 283–291.